

The Plutino population: An Abundance of contact binaries.

Audrey Thirouin¹

Lowell Observatory, 1400 W Mars Hill Rd, Flagstaff, Arizona, 86001, USA.

thirouin@lowell.edu

and

Scott S. Sheppard²

Department of Terrestrial Magnetism (DTM), Carnegie Institution for Science, 5241 Broad Branch Rd. NW, Washington, District of Columbia, 20015, USA.

ssheppard@carnegiescience.edu

ABSTRACT

We observed twelve Plutinos over two separated years with the 4.3m Lowell’s Discovery Channel Telescope. Here, we present the first lightcurve data for those objects. Three of them (2014 JL₈₀, 2014 JO₈₀, 2014 JQ₈₀) display a large lightcurve amplitude explainable by a single elongated object, but are most likely caused by a contact binary system due to their lightcurves morphology. These potential contact binaries have rotational periods from 6.3 h to 34.9 h and peak-to-peak lightcurve variability between 0.6 and 0.8 mag. We present partial lightcurves allowing us to constrain the lightcurve amplitude and the rotational period of another nine Plutinos. By merging our data with the literature, we estimate that up to ~40% of the Plutinos could be contact binaries. Interestingly, we found that all the suspected contact binaries in the 3:2 resonance are small with absolute magnitude $H > 6$ mag. Based on our sample and the literature, up to ~50% of the small Plutinos are potential contact binaries.

Subject headings: Kuiper Belt Objects: 1995 HM₅, 2001 KB₇₇, 2006 UZ₁₈₄, 2014 JK₈₀, 2014 JL₈₀, 2014 JO₈₀, 2014 JP₈₀, 2014 JQ₈₀, 2014 JT₈₀, 2014 KC₁₀₂, 2014 KX₁₀₁, 2015 BA₅₁₉, Techniques: photometric

1. Introduction

Any object confined in a mean motion resonance with Neptune receive the name of *resonant object*. At ~39.4 AU, the 2:3 resonance is the most stable and densely populated resonance (Chiang & Jordan 2002; Jewitt et al. 1998). As Pluto is a 3:2 resonant object, all bodies trapped into this resonance receive the denomination of *Plutinos*. According to Malhotra (1995), some Plutinos cross Neptune’s orbit, but they never suffer a close approach. The overabundance of Plutinos is likely due to Neptune’s migration (Malhotra 1993, 1995). Neptune could have been created in the Inner Solar System and migrated outwards to its actual location, due to angular momentum exchange

with surrounding planetesimals (Fernandez & Ip 1984). With Neptune’s migration, the resonances moved into the trans-Neptunian belt and the planetesimals were captured by such resonances (Levison et al. 2008; Malhotra 1995). In conclusion, the migration and circularization of this planet’s orbit provoked the capture of objects into the resonances. A migration of ~8 AU over 10^7 years reproduces the observed distribution of Plutinos (Gomes 2000).

Several of the largest Plutinos are binaries or multiple systems: Pluto-Charon (and 4 smaller moons), Huya (formerly 2000 EB₁₇₃), Orcus-Vanth (2004 DW), Lempo (1999 TC₃₆, triple system), and 2003 AZ₈₄. These binaries are likely formed by collisional impact on the pri-

mary. Trapped in the Plutinos, Mors-Somnus (2007 TY₄₃₀) is a noteworthy equal-sized wide system that cannot have been created by impact, and is like a dynamically Cold Classical equal-sized binary (Sheppard et al. 2012). Finally, 2001 QG₂₉₈ is a near equal-sized contact binary (Sheppard & Jewitt 2004). Therefore, less than 3% of the Plutinos are known binaries. The Plutino population seems to have a deficit in separated wide binary systems compared to the other dynamical groups (Noll et al. 2008; Compère et al. 2013). As said in Thirouin et al. (2017), contact binaries are unresolved with the *Hubble Space Telescope* (*HST*). These compact systems may remain undiscovered and therefore the current fraction of close/compact binary systems in the Plutino population and other populations by extension are unknown. Similarly, as argued by Porter & Grundy (2012), there is potentially a large fraction of binaries with circular and very tight orbit due to Kozai effects that are undetectable with *HST*. Even if it is still unclear how contact binaries are formed, one can argue that tidal effects as suggested by Porter & Grundy (2012) can create very tight orbits, but the gravitational collapse is also an option (Nesvorný et al. 2010). Finally, as suggested by the star formation theory, if a triple system loses one component, the other two objects have to shrink their orbit to go back to a stable configuration and can potentially create a contact/close binary (Bodenheimer 2011). However, it is important to point out that several of these models are not dedicated to the TNO science, and that we are still missing several observables to infer if a model is working or not. We aim that our work regarding contact binaries will help to constrain their localizations, characteristics, fraction among other properties that can be used for modeling or as observables to check the validity of a model.

2. Data reduction, analysis, and results

Data obtained between May and July 2017, and November-December 2015 with the Lowell Observatory’s 4.3 m Discovery Channel Telescope (DCT) are presented. We used exposure times of 300 to 500 seconds with a broad-band filter with the Large Monolithic Imager (LMI) (Levine et al. 2012). Details about the telescope and instrument can be found in Thirouin et al. (2017). The ob-

serving log is in Table 1.

The data reduction and analysis is the same as in our previous works, but following we summarize the main steps. Images were biased subtracted and flatfielded thanks to calibration images obtained each night (dome and/or twilight flats depending on the weather conditions). Then, we proceed with the aperture photometry with a data reduction software using the Daophot routines described in Stetson (1987). The optimal aperture radius in order to estimate the flux of the object and limit the background contamination has been estimated by a growth curve (Stetson 1990; Howell 1989). We selected 20 stars per field as reference stars. We also played with the pointings in order to keep about the same field of view every night and thus the same reference stars or at least keep a couple of reference stars in common between pointings. Such a technique allows us to use the same reference stars across observing runs and also allow us to merge our datasets. The error associated to the photometry has been estimated following the formalism in Howell (1989). Finally, we looked for periodicities using the Lomb periodogram technique (Lomb 1976; Press et al. 1992), and double-checked our results with the Phase Dispersion Minimization from Stellingwerf (1978). More details about our data reduction/analysis procedures are available in Thirouin et al. (2010, 2012); Thirouin (2013).

In this section, we show our photometric results for our partial and complete lightcurves. All our lightcurves with a rotational period estimate are plotted over two cycles. In case of partial lightcurve without rotational period estimate, the photometry with error bars is plotted versus Julian Date (no light-time correction applied). We summarize our photometry in Appendix A, and our results are reported in Table 2.

It is important to point out that our study was designed to constrain the percentage of large amplitude objects in the Plutino population. Therefore, if an object was not showing obvious sign of large variability characteristic of a contact binary, we stop observing it. But, in some cases our observations were interrupted due to bad weather and/or smoke. In conclusion, for the rest of our study, all objects with an observed variability smaller than 0.2 mag will be considered as a non contact binary.

2.1. Lightcurves of potential contact binaries

Now, the lightcurves of 2014 JL₈₀, 2014 JO₈₀, and 2014 JQ₈₀ are displayed. All of these objects present a large variability between 0.55 and 0.76 mag, and rotational periods from 6.32 h up to almost 35 h. These objects will be analyzed in detail in Section 3.

2.1.1. 2014 JL₈₀

With H=7.1 mag as absolute magnitude according to the Minor Planet Center (MPC), we estimate a size of 253/113 km (geometric albedo of 0.04/0.20).

After two nights of observations of 2014 JL₈₀, a very long rotational period of more than 24 h, and a large variability were suspected. Three more nights with sparse sampling observations were required to present a potential lightcurve. The highest peak of the Lomb periodogram corresponding to the single-peaked lightcurve is located at 1.38 cycles/day (17.44 h, Figure 1). Assuming a double-peaked lightcurve, the rotational period is 34.87 h. Such a slow rotation means that 2014 JL₈₀ is one of the few slow rotators detected from ground-based observations with Pluto/Charon and 2010 WG₉ (Rabinowitz et al. 2013; Buie et al. 1997). In Figure 1, we plot the corresponding lightcurve with a variability of 0.55 mag. Unfortunately, we do not have the U-shape of the curve, but the V-shape of the second minima is visible. It is important to point out that the lightcurve of 2014 JL₈₀ is very sparse and thus the rotational period estimate needs to be improved. In Figure 1, one can appreciate that there are several aliases of the main peak located at 2.37 cycles/day (10.11 h) and 0.77 cycles/day (31.03 h). In all cases, the rotation of 2014 JL₈₀ is very slow. For the purpose of the following work, we will use the main peak as rotational period estimate.

A test using the full-width-at-half-maximum (FWHM) of the lightcurve's peaks can suggest if an object is potentially a close binary or an elongated object (Thirouin & Sheppard 2017). In fact, by estimating the FWHM of the peaks, we have shown that the FWHM of the peaks are different in case of single and contact binary objects using their lightcurve plotted as magnitude ver-

sus rotational phase. Unfortunately, because the lightcurve of 2014 JL₈₀ is sparse sampled, we are not able to provide an estimate for the U- and V-FWHM. But, based on the slow rotation of this object we can argue that tidal effects due to a companion have affected the rotational period of this object (Thirouin et al. 2014). In fact, several TNOs (Pluto-Charon (Buie et al. 1997), Sila-Nunam (Grundy et al. 2012), and maybe 2010 WG₉ (Rabinowitz et al. 2013)) have rotational periods longer than a day and are synchronously locked binaries.

Following the procedure described in Rabinowitz et al. (2013), and assuming that 2014 JL₈₀ is an equal-sized binary system, we can estimate the separation between the two components. With a primary and a secondary having comparable diameters of 150 km, a density of 1000 kg m⁻³, we calculate a ~320 km separation. Such a separation is below the resolution of the *Hubble Space Telescope* (Noll et al. 2008).

Because of the large variability and the second minima shape, 2014 JL₈₀ is likely a contact binary or nearly contact binary and this case will be discussed in the following section.

2.1.2. 2014 JO₈₀

The absolute magnitude of 2014 JO₈₀ is 7.4 mag (MPC value), thus the diameter is 220/98 km using an albedo of 0.04/0.20.

With four nights of data, the Lomb periodogram favors a peak at 7.59 cycles/day (3.16 h, Figure 2). There are also aliases of the main peak located at 6.58 cycles/day (3.65 h) and 8.58 cycles/day (2.80 h). All techniques used to confirm the periodicity favors the main peak and thus we are using this value for our work. Because of the large amplitude and because of an asymmetry of about 0.1 mag between the peaks, we favor the double-peaked lightcurve with a rotational period of 6.32 h. The variability is 0.60±0.05 mag (Figure 2).

Following Thirouin & Sheppard (2017), we estimate the U-FWHM at 0.38 and 0.37, and the V-FWHM at 0.16. Therefore, 2014 JO₈₀ presents the same characteristic as the likely contact binaries reported in Thirouin & Sheppard (2017).

2.1.3. 2014 JQ₈₀

Based on the MPC estimate, the absolute magnitude of 2014 JQ₈₀ is 7.0 mag, suggesting a diameter of 265/118 km with an albedo of 0.04/0.20.

With a total of 83 images obtained over two months in 2017, we report the first and unique lightcurve of 2014 JQ₈₀. The Lomb periodogram, and the PDM technique favor a rotational period of 3.97 cycles/day (6.08 h, Figure 3), but there two aliases of this main peak with lower confidence levels at 2.95 cycles/day (8.13 h) and 4.94 cycles/day (4.86 h). Following, we will use the main peak with the highest confidence level as the rotational periodicity. Because of the large amplitude of this object, we favor the double-peaked lightcurve with a rotational period of 12.16 h. The lightcurve amplitude is 0.76 ± 0.04 mag (Figure 3).

With the U-FWHM of 0.34 and 0.35, and the V-FWHM of 0.16 and 0.13, 2014 JQ₈₀ meets the criteria mentioned in Thirouin & Sheppard (2017) for likely contact binaries.

Our study regarding the U-/V-FWHM is summarized in Figure 4. A complete description of this plot is available in Thirouin & Sheppard (2017).

2.2. Partial lightcurves

2.2.1. 1995 HM₅

1995 HM₅ is the smallest object in our sample. With an absolute magnitude of 7.7 mag, its diameter is between 86 and 192 km assuming a geometric albedo of 0.04 and 0.2, respectively. We report about 0.6 h of observations obtained in May 2017. Our few observations show a minimum variability of ~ 0.1 mag (Figure 5). Based on our data, no rotational period is derived.

2.2.2. (469362) 2001 KB₇₇

We report 6 images of 2001 KB₇₇ obtained on UT 18 June. In about 4 h, 2001 KB₇₇ displays a variability of 0.15 mag (Figure 5). To our knowledge, there is no bibliographic reference to compare our result with. No rotational period is derived from our observations, we can only constrain the period to be longer than 4 h.

2.2.3. 2006 UZ₈₄

We observed 2006 UZ₁₈₄ over two consecutive nights in November-December 2015. Unfortunately, due to bad weather conditions, only 10 images were usable. Over two nights, this object seems to have a variability of about 0.2 mag, and no period is derived (Figure 5).

2.2.4. 2014 JK₈₀

2014 JK₈₀ was studied over two consecutive nights at the end of June 2017. Data from the first night are not showing an obvious sign of variability, but the second night shows a variability of about 0.17 mag (Figure 5).

2.2.5. 2014 JP₈₀

2014 JP₈₀, with H=4.9 mag, a diameter of 698/311 km considering an albedo of 0.04/0.2 is the largest object here. With only 5 images obtained over about 0.5 h, it is difficult to provide any reliable conclusion regarding 2014 JP₈₀. The partial lightcurve shows a variability of ~ 0.1 mag (Figure 5).

2.2.6. 2014 JT₈₀

We have five images of 2014 JT₈₀ obtained over about 1 h in June 27, but only 3 images were usable. The variability is about 0.1 mag (Figure 5).

2.2.7. 2014 KC₁₀₂

We have two nights of data for 2014 KC₁₀₂. The second night shows the maximum of the curve with a variability of around 0.2 mag over 4.5 h of observations (Figure 5). Therefore, considering a double-peaked lightcurve, we suggest a rotational period of about 9 h, but more data are needed for a better estimate.

2.2.8. 2014 KX₁₀₁

We report two consecutive nights of observations for 2014 KX₁₀₁. Both nights are showing a variability of about 0.2 mag (Figure 5). Unfortunately, no rotational period estimate is derived.

2.2.9. 2015 BA₅₁₉

2015 BA₅₁₉ was observed during only one night on UT May 1. In a couple of hours of observations,

a variability of ~ 0.16 mag is noticed. The partial lightcurve plotted in Figure 5 presents one maximum and one minimum, so the rotational period of this object should be approximately 8 h (assuming a double-peaked lightcurve). No additional information about this object has been found in the literature.

3. Analysis

Next, we consider a contact binary configuration and a single very elongated object option to explain the high lightcurve variability of 2014 JL₈₀, 2014 JO₈₀, and 2014 JQ₈₀.

3.1. Roche system

The large lightcurve amplitude of 2014 JL₈₀, 2014 JO₈₀, and 2014 JQ₈₀ are best explained if these objects are contact binary systems. Following, we constrain basic information about the systems Leone et al. (1984). We estimate the mass ratio and the density using the Roche sequences (Figure 7). Following Leone et al. (1984) assumptions, we derive min and max cases. The density range in Leone et al. (1984) is limited to $\rho=1000 \text{ kg m}^{-3}$ - 5000 kg m^{-3} , but lower densities are possible for the TNOs.

3.1.1. 2014 JL₈₀

For 2014 JL₈₀, based on Leone et al. (1984) we estimate that $q_{min} \sim q_{max} \sim 0.5$, whereas the density range is $\rho_{min}=1000 \text{ kg m}^{-3}$, $\rho_{max}=5000 \text{ kg m}^{-3}$.

Considering 2014 JL₈₀ as a binary with a mass ratio of 0.5, and a density of 1000 kg m^{-3} , the axis ratios of the primary are: $b/a=0.99$, $c/a=0.98$ ($a=71/31 \text{ km}$, $b=71/31 \text{ km}$, and $c=70/31 \text{ km}$ assuming an albedo of 0.04/0.2), the axis ratios of the secondary are: $b_{sat}/a_{sat}=0.98$, $c_{sat}/a_{sat}=0.97$ ($a_{sat}=57/26 \text{ km}$, $b_{sat}=56/26 \text{ km}$, and $c_{sat}=55/25 \text{ km}$ with an albedo of 0.04/0.2). The parameter D is 0.34, thus the distance between bodies is 378/169 km (albedo of 0.04/0.2).

3.1.2. 2014 JO₈₀

For 2014 JO₈₀, we have: i) a system with $q_{min}=0.3$ and $\rho_{min}=3.25 \text{ g cm}^{-3}$ or ii) a system $q_{max}=0.42$ and $\rho_{max}=5 \text{ g cm}^{-3}$. Based on the lightcurve amplitude, the uncertainty for the mass ratio is ± 0.07 . If 2014 JO₈₀ is a binary

system with a mass ratio of 0.3, and a density of 3.25 g cm^{-3} , we derive the axis ratios of the primary: $b/a=0.90$, $c/a=0.81$ ($a=75/33 \text{ km}$, $b=68/30 \text{ km}$, and $c=61/27 \text{ km}$ assuming an albedo of 0.04/0.2), the axis ratios of the secondary: $b_{sat}/a_{sat}=0.46$, $c_{sat}/a_{sat}=0.43$ ($a_{sat}=79/36 \text{ km}$, $b_{sat}=36/16 \text{ km}$, and $c_{sat}=34/15 \text{ km}$ assuming an albedo of 0.04/0.2). The separation between the components is 175/78 km with an albedo of 0.04/0.2, assuming $D=0.88$.

3.1.3. 2014 JQ₈₀

For 2014 JQ₈₀, we compute two extreme options: i) a system with $q_{min}=0.57$ and $\rho_{min}=1 \text{ g cm}^{-3}$ or ii) a system with $q_{max}=0.92$ and $\rho_{max}=5 \text{ g cm}^{-3}$. Following, we will consider conservative mass ratio of $q_{min}=0.6$.

If 2014 JQ₈₀ is a binary with $q=0.6$, and $\rho=1 \text{ g cm}^{-3}$, we obtain for the primary: $b/a=0.86$, $c/a=0.79$ ($a=84/37 \text{ km}$, $b=72/32 \text{ km}$, and $c=66/29 \text{ km}$ assuming an albedo of 0.04/0.2), for the secondary: $b_{sat}/a_{sat}=0.75$, $c_{sat}/a_{sat}=0.69$ ($a_{sat}=78/35 \text{ km}$, $b_{sat}=59/26 \text{ km}$, and $c_{sat}=54/24 \text{ km}$ assuming an albedo of 0.04/0.2). The separation between the components is 208/92 km with an albedo of 0.04/0.2 and $D=0.78$.

The typical density in the Kuiper belt is $\sim 1 \text{ g cm}^{-3}$, with the exceptions of a few denser bigger objects (Thirouin et al. 2016; Vilenius et al. 2014; Brown 2013; Grundy et al. 2012; Sheppard et al. 2008). Therefore, previously we do not derive axis ratios and separation assuming a high density $\rho_{max}=5 \text{ g cm}^{-3}$. It is important to point out that a careful modelling of these systems using several lightcurves obtained a different epochs will be necessary to derive accurate basic parameters for all of them.

3.2. Jacobi ellipsoid

The lightcurves of 2014 JL₈₀, 2014 JO₈₀, and 2014 JQ₈₀ are not reproduced by a second order Fourier series fit because of their U-/V-shapes. Therefore, we favor the option of contact binary to explain these lightcurves, but if these objects are single Jacobi ellipsoids, we can constrain their elongations, and densities (Thirouin et al. 2017; Thirouin & Sheppard 2017).

3.2.1. 2014 JL₈₀

In the case of 2014 JL₈₀, considering a viewing angle of 90°, we find $a/b=1.67$, and $c/a=0.44$ (Chandrasekhar 1987). So, we compute: $a=213$ km ($a=95$ km), $b=128$ km ($b=57$ km), and $c=94$ km ($c=42$ km) for an albedo of 0.04 (0.20) and an equatorial view. Using a viewing angle of 60°, we derive an axis ratio $a/b>2.31$. As ellipsoids with $a/b>2.31$ are unstable to rotational fission, the viewing angle of 2014 JL₈₀ must be larger than 62.5° (Jeans 1919). With an equatorial view, the density is $\rho\geq 0.04$ g cm⁻³. The very long rotation of 2014 JL₈₀ likely means that this object cannot be a Jacobi ellipsoid which generally are fast rotators and have high angular momentum (Sheppard et al. 2008).

3.2.2. 2014 JO₈₀

Assuming an equatorial view, we compute $a/b=1.72$, and $c/a=0.42$. Therefore, the axis are: $a=170$ km ($a=85$ km), $b=99$ km ($b=49$ km), and $c=71$ km ($c=36$ km) for an albedo of 0.04 (0.20) and an equatorial view. As for 2014 JL₈₀, a viewing angle of 60° suggests that 2014 JO₈₀ is unstable to rotational fission. We estimate that the aspect angle is between 65° and 90°. Using an equatorial view, the density is $\rho\geq 1100$ kg m⁻³. The very short period of 2014 JO₈₀ makes a Jacobi type object likely because of its high angular momentum.

3.2.3. 2014 JQ₈₀

With an equatorial view for 2014 JQ₈₀, we obtain $a/b=2$, and $c/a=0.38$. Therefore, we compute: $a=248$ km ($a=111$ km), $b=124$ km ($b=55$ km), and $c=94$ km ($c=42$ km) for an albedo of 0.04 (0.20) and an equatorial view. 2014 JQ₈₀ is stable to rotational fission if its viewing angle is larger than 74°. Assuming $\xi=90^\circ$, the density is $\rho\geq 0.32$ g cm⁻³.

In conclusion, to explain the morphology of the lightcurves of 2014 JL₈₀, 2014 JO₈₀, and 2014 JQ₈₀, we showed details of a single elongated object or close binary configuration. However, because of the V-/U-shape, and the extreme variability, we favor the contact binary explanation. Future observations are required to infer the nature of 2014 JL₈₀, 2014 JO₈₀, and 2014 JQ₈₀. It

is also important to point out that we used the rotational periods favored by the main peaks (i.e. peak with the highest confidence level), however more data can be useful to favor such peaks and not some of the aliases.

4. Percentage of contact binaries

4.1. Status of the Plutino lightcurve studies

In Table 2, and Table 3 are summarized the short-term variability studies of Plutinos published in this work, and in the literature (respectively). In total, 39 Plutinos¹ have been observed for lightcurves: 12 Plutinos are reported in this paper and 27 in the literature. However, only 21 objects have a rotational period (secure result and tentative), the rest have only lightcurve amplitude constraints.

Based on Table 3, one can appreciate that most of the Plutinos display a low lightcurve amplitude with a mean value of ~ 0.13 mag (Figure 8). But, several objects are showing larger variability: Pluto, Arawn (1994 JR₁), 1995 QY₉, 2000 GN₁₇₁, and 2001 QG₂₉₈. The NASA's New Horizons flyby of Pluto confirmed that the lightcurve amplitude is due to a strong albedo contrast on Pluto's surface, whereas 2001 QG₂₉₈ is a contact binary (Buratti et al. 2017; Sheppard & Jewitt 2004). Arawn, also observed by New Horizons at a very high phase angle, displays an amplitude of 0.58 mag² based on the fit reported in Porter et al. (2016). We estimate the V-FWHM and the U-FWNM of Arawn and find that the U-FWHM and the V-FWHM are about the same (~ 0.26). Therefore, following the criteria reported in Thirouin & Sheppard (2017), Arawn is likely not a contact binary, and thus its large amplitude is due to an elongated shape. However, the Arawn observations were performed at a phase angle up to $\sim 59^\circ$ whereas the typical ground-based TNO lightcurves are obtained at a phase angle up to $\sim 2^\circ$. With such a high phase angle compared to Earth observations, it is difficult to directly compare the lightcurve morphologies

¹To date, 225 Plutinos are known. So, based on published results, only $\sim 17\%$ of the Plutinos have been observed for lightcurves.

²Porter et al. (2016) reported an amplitude of 0.8 mag, being the difference between the highest and lowest point of the curve.

as shadowing effect is not negligible. Therefore, the direct comparison of ground- and space-based lightcurves can be wrong. In the case of 1995 QY₉, only one lightcurve is reported in the literature (Romanishin & Tegler 1999). The lightcurve amplitude is about 0.6 mag. Unfortunately, no further study of this object can confirm or not such finding, and we cannot use the V-/U-FWHM technique as the photometry is not available and the lightcurve plotted is not phased folded.

The lightcurve of 2000 GN₁₇₁ displays a large variability of ~ 0.6 mag (Sheppard & Jewitt 2002; Rabinowitz et al. 2007). It has been suggested that the lightcurve of 2000 GN₁₇₁ is due to an elongated shape, but the option of a contact binary system was not excluded (Sheppard & Jewitt 2002). Later, based on lightcurve modeling Lacerda & Jewitt (2007) suggested that the Roche and Jacobi solution are equivalent, and thus could not favor any option regarding the nature of this object/system. Using Sheppard & Jewitt (2002) lightcurve, we estimate an U-FWHM of 0.33 and a V-FHWM of 0.22 and 0.19, therefore according to our study reported in Thirouin & Sheppard (2017), 2000 GN₁₇₁ is likely a contact binary (Figure 4). The most recent lightcurve of 2000 GN₁₇₁ was obtained in 2007 (Dotto et al. 2008). They obtained a rotational period consistent with Sheppard & Jewitt (2002) result, and they argue that the lightcurve amplitude is also similar. However, based on their Figure 3, the lightcurve amplitude is smaller than reported. Their photometry is not available online, but using their plot, the amplitude seems to be around 0.53 mag. In conclusion, there is a potential change in the lightcurve amplitude and thus potentially a change in the system orientation between the first and last lightcurve obtained in 2001 and 2007. A careful modeling of those lightcurves may infer the nature of the system/object.

In conclusion, 2000 GN₁₇₁ is likely a contact binary and a change in the lightcurve amplitude is potentially observable. In the case of 1995 QY₉, a new lightcurve will be useful to constrain the nature of this object. For the purpose of our following study, we will assume that this object is a single elongated one, as it is the case for Arawn.

4.2. Fraction of contact binaries in the Plutino population

With the literature and this work, we have evidence that 5 likely/confirmed contact binaries are in the Plutino population, not including the large amplitude objects 1995 QY₉ and Arawn as we assume they are elongated but not contact binary. We want to point out that these 5 likely/confirmed contact binaries are based on the literature data and the objects observed for this work (i.e. 5 out of 39 objects). Such a number seems to indicate that the Plutino population may have a large reservoir of contact binaries compared to the other populations (Thirouin & Sheppard 2017; Thirouin et al. 2017; Lacerda et al. 2014; Sheppard & Jewitt 2004). It is important to point out that a threshold of 0.9 mag has been used in the literature to identify a contact binary, but a non-equal-sized close system may never pass such a threshold even if observed equator-on. Therefore, in the next paragraphs we will use several lightcurve amplitude limits. We also assume that the partial lightcurves reported in this work are due to non-contact binary objects. However, some of them are maybe contact binary with very long rotational period and thus their identification is not possible based on our data. Therefore, the fractions of contact binaries reported below are lower limits.

Following the procedure detailed in Sheppard & Jewitt (2004), we calculate the percentage of close binaries in the Plutino population.

In first approximation, we assume that the lightcurve amplitude of an object with axes $a > b$, and $b = c$ varies following:

$$\Delta_m = 2.5 \log \left(\frac{1 + \tan \theta}{(b/a) + \tan \theta} \right) \quad (1)$$

θ is the angle of the object's pole relative to the perpendicular of the sight line. An amplitude of 0.9 mag is reached at $\theta = 10^\circ$ for an object with an elongation of $a/b = 3$. Therefore, the probability to observe an object from a random distribution within 10° from the sight line is $P(\theta \leq 10^\circ) = 0.17$. With the same approach, we estimate that an amplitude of 0.5 mag is reached at $\theta = 36^\circ$, whereas an amplitude of 0.6 mag is reached at $\theta = 27^\circ$, and an amplitude of 0.7 mag is reached at $\theta = 20^\circ$. In our sample of 12 objects we have one TNO with a $\Delta_m \geq 0.7$ mag. So

the detection of one TNO with $\Delta_m \geq 0.7$ mag implies that the abundance of similar objects is: $f(\Delta_m \geq 0.7 \text{ mag}) \sim 1/(12 * P(\theta \leq 20^\circ)) \sim 25\%$. Similarly, we estimate: $f(\Delta_m \geq 0.6 \text{ mag}) \sim 2/(12 * P(\theta \leq 27^\circ)) \sim 37\%$, and $f(\Delta_m \geq 0.5 \text{ mag}) \sim 3/(12 * P(\theta \leq 36^\circ)) \sim 42\%$. Using our sample and the literature, we calculate: $f(\Delta_m \geq 0.7 \text{ mag}) \sim 28\%$, $f(\Delta_m \geq 0.6 \text{ mag}) \sim 42\%$, and $f(\Delta_m \geq 0.5 \text{ mag}) \sim 40\%$. These estimates do not include 1995 QY₉ and Arawn as we assume they are elongated objects.

In a second approximation, and assuming a triaxial Jacobi with $a \geq b = c$, the lightcurve variability is (Sheppard & Jewitt 2004):

$$\Delta_m = 2.5 \log \left(\frac{a}{b} \right) - 1.25 \log \left(\left(\left(\frac{a}{b} \right)^2 - 1 \right) \sin^2 \theta + 1 \right) \quad (2)$$

With the same approach as previously, we find for our sample: $f(\Delta_m \geq 0.7 \text{ mag}) \sim 19\%$, $f(\Delta_m \geq 0.6 \text{ mag}) \sim 34\%$, $f(\Delta_m \geq 0.5 \text{ mag}) \sim 44\%$. With the literature and our sample, we compute: $f(\Delta_m \geq 0.7 \text{ mag}) \sim 22\%$, $f(\Delta_m \geq 0.6 \text{ mag}) \sim 39\%$, $f(\Delta_m \geq 0.5 \text{ mag}) \sim 42\%$. It is important to mention that we are considering that the sparse lightcurves with low to moderate amplitude reported here are due to single objects. In some cases our temporal coverage is limited and some objects may be contact binaries with very slow rotation as 2014 JL₈₀. Therefore, our estimates are lower limits.

Ten objects in our sample have absolute magnitude $H \geq 7.0$ mag (diameter of 265/118 mag with albedo of 0.04/0.2). So far, observers have been focusing on large and bright TNOs, with only a handful of studies of smaller objects (see Thirouin (2013) for a complete review). Therefore, we are testing a new size range of objects, and only little information is known about rotational properties of medium to small TNOs. In Figure 8, one can appreciate that the lightcurve amplitude is increasing at higher absolute magnitude (i.e. small objects). Therefore, we decide to test the percentage of high amplitude objects for smaller size. We follow the same approach as previously, but we now only focus on objects with $H \geq 6.0$ mag (diameter of 419/188 mag assuming an albedo of 0.04/0.2). Based on our sample and the literature, we have: $f(\Delta_m \geq 0.7 \text{ mag}) \sim 35\%$, $f(\Delta_m \geq 0.6 \text{ mag}) \sim 52\%$, and $f(\Delta_m \geq 0.5 \text{ mag}) \sim 50\%$

using Equation 1. With Equation 2, we have: $f(\Delta_m \geq 0.7 \text{ mag}) \sim 27\%$, $f(\Delta_m \geq 0.6 \text{ mag}) \sim 48\%$, and $f(\Delta_m \geq 0.5 \text{ mag}) \sim 52\%$. In conclusion, $\sim 40\%$ of the Plutinos and $\sim 50\%$ of the small Plutinos could be contact binaries using a cut-off at $\Delta_m \geq 0.5$ mag.

Several studies mentioned that there is an anti-correlation between size and lightcurve amplitude (Thirouin et al. 2010; Thirouin 2013; Benecchi & Sheppard 2013). In other words, at smaller sizes (i.e. larger absolute magnitude), the lightcurve amplitude is larger suggesting that the small objects are more elongated and have more irregular shape. Such a tendency have been reported in all the dynamical group of TNOs (Thirouin 2013). Therefore, one may expect that objects reported in this work are likely more elongated/deformed, however, their lightcurves are showing the U-/V-shapes indicatives of contact binary, and therefore the contact binary option is more likely.

4.3. Correlation/anti-correlation search

We also search for correlation/anti-correlation between the lightcurve amplitude and the rotational period with the orbital elements (technique detailed in Thirouin et al. (2016)). Only two strong trends have been identified (Figure 8): the lightcurve amplitude is correlated with the absolute magnitude ($\rho = 0.544$, significance level = 98%), and an anti-correlation between lightcurve amplitude and inclination ($\rho = -0.505$, significance level = 97%). The correlation between amplitude and size suggesting that the smaller objects present a large variability has been already noticed in several works and seems to be present in all the TNO dynamical groups (Sheppard et al. 2008; Benecchi & Sheppard 2013; Thirouin 2013). The anti-correlation between amplitude and inclination suggests that the variable objects are at low inclination. Such a trend has been noticed in several sub-populations of TNOs (Thirouin 2013). However, it is interesting that the large amplitude objects are located at low inclination in the Plutino population. Sheppard (2012) concluded that the 3:2 population presents a large variety of colors from neutral to ultra-red, suggesting a Cold Classical component at low inclination. Unfortunately, we do not have color studies for our objects to identify them as ultra-red objects (i.e. as a cold classical TNO) or not. However, color studies are available for 2001 QG₂₉₈ and 2000 GN₁₇₁ (Shep-

pard & Jewitt 2002, 2004). With a B-R of 1.6 mag for 2001 QG₂₉₈ and 1.55 mag for 2000 GN₁₇₁, both objects are very red. Typical error bars are ± 0.04 mag, and thus taking into account this uncertainty, both objects are potentially ultra-red. In conclusion, both objects are potentially presenting similar characteristics as the dynamical Cold Classical TNOs. By studying the contact binaries in the Plutino and the Cold Classical populations, one will be able to check if both populations share the same binary fraction and characteristics, if there was some leakage of objects between the two populations, and constrain Neptune’s migration (paper in preparation).

5. Conclusions

We have displayed data of twelve Plutinos over two years using the Lowell’s Discovery Channel Telescope. An homogeneous dataset reduced and analyzed the same way is presented. Our findings can be summarized as:

- For nine objects, we report partial lightcurves showing a typical variability lower than 0.2 mag. Three objects in our sample of 12 are showing a lightcurve amplitude larger than 0.5 mag (25% of our sample). 2014 JL₈₀ is the slowest rotator in our sample with a period of 34.87 h and an amplitude of 0.55 mag. The period of 2014 JO₈₀ is 6.32 h and the amplitude is 0.60 mag. In the case of 2014 JQ₈₀, the lightcurve amplitude is 0.76 mag and the rotational period is 12.16 h. Lightcurves of 2014 JL₈₀, and 2014 JQ₈₀ display a U- and V-shape indicating contact binaries. In the case of the very slow rotator 2014 JL₈₀, the V-shape seems to be present, but unfortunately, we do not have the U-shape of the curve in our data.
- The large amplitude lightcurves are best explained by contact binary systems, but single very elongated objects cannot be ruled out. Assuming a contact binary configuration, we derive $q=0.5$, and a density of 1 g cm^{-3} for 2014 JL₈₀, a $q=0.3$ and a density of 3.25 g cm^{-3} for 2014 JO₈₀, and $q=0.6$ with a density of 1 g cm^{-3} for 2014 JQ₈₀.
- Thanks to this study, the current population

of likely/confirmed contact binaries is composed of 8 TNOs: 1 dynamically Cold Classical object (Thirouin & Sheppard 2017), 1 in the Haumea family (Lacerda et al. 2014), 1 in the 5:2 mean motion resonance (Thirouin et al. 2017) and 5 in the Plutino population (this work, and Sheppard & Jewitt (2002, 2004)).

- Based on our sample, we estimate the fraction of contact binaries in the Plutino population. Using a cut-off of 0.5 mag, we find that $\sim 40\%$ of the Plutinos can be contact binaries. Interestingly, all the known contact binaries in the Plutino population are small with absolute magnitude $H \geq 6$ mag. We estimate a contact binary fraction of about 50% for the small Plutinos. This suggests the Plutino population may have significantly more contact binaries than other TNO populations. Future observations of smaller objects in other TNO populations are needed to confirm (or not) this finding.

Authors thank an anonymous referee for helpful comments and corrections. This research is based on data obtained at the Lowell Observatory’s Discovery Channel Telescope (DCT). Lowell operates the DCT in partnership with Boston University, Northern Arizona University, the University of Maryland, and the University of Toledo. Partial support of the DCT was provided by Discovery Communications. LMI was built by Lowell Observatory using funds from the National Science Foundation (AST-1005313). We acknowledge the DCT operators: Andrew Hayslip, Heidi Larson, Teznie Pugh, and Jason Sanborn. A. Thirouin is partly supported by Lowell Observatory. Authors acknowledge support from the National Science Foundation, and the grant awarded to the “Comprehensive Study of the Most Pristine Objects Known in the Outer Solar System” (AST-1734484).

REFERENCES

- Benecchi, S. D., & Sheppard, S. S. 2013, *AJ*, 145, 124
- Binzel, R. P., Farinella, P., Zappala, V., & Cellino, A. 1989, *Asteroids II*, 416

- Bodenheimer, P. H. 2011, *Principles of Star Formation: , Astronomy and Astrophysics Library*. ISBN 978-3-642-15062-3. Springer-Verlag Berlin Heidelberg, 2011,
- Brown, M. E. 2001, *AJ*, 121, 2804
- Brown, M. E. 2013, *ApJ*, 778, L34
- Buie, M. W., Tholen, D. J., & Wasserman, L. H. 1997, *Icarus*, 125, 233
- Chandrasekhar, S. 1987, New York : Dover, 1987.
- Buratti, B. J., Hofgartner, J. D., Hicks, M. D., et al. 2017, *Icarus*, 287, 207
- Chiang, E. I., & Jordan, A. B. 2002, *AJ*, 124, 3430
- Collander-Brown, S. J., Fitzsimmons, A., Fletcher, E., Irwin, M. J., & Williams, I. P. 1999, *MNRAS*, 308, 588
- Compère, A., Farrelly, D., Lemaître, A., & Hestroffer, D. 2013, *A&A*, 558, A4
- Davies, J. K., McBride, N., & Green, S. F. 1997, *Icarus*, 125, 61
- Degewij, J., Tedesco, E. F., & Zellner, B. 1979, *Icarus*, 40, 364
- Dotto, E., Perna, D., Barucci, M. A., et al. 2008, *A&A*, 490, 829
- Elliot, J. L., Kern, S. D., Clancy, K. B., et al. 2005, *AJ*, 129, 1117
- Fernandez, J. A., & Ip, W.-H. 1984, *Icarus*, 58, 109
- Galiazzo, M., de la Fuente Marcos, C., de la Fuente Marcos, R., et al. 2016, *Ap&SS*, 361, 212
- Gladman, B., Marsden, B. G., & Vanlaerhoven, C. 2008, *The Solar System Beyond Neptune*, 43
- Gomes, R. S. 2000, *AJ*, 120, 2695
- Grundy, W. M., Benecchi, S. D., Rabinowitz, D. L., et al. 2012, *Icarus*, 220, 74
- Howell, S. B. 1989, *PASP*, 101, 616
- Jeans, J. H. 1919, Cambridge, University press, 1919.
- Jewitt, D., Luu, J., & Trujillo, C. 1998, *AJ*, 115, 2125
- Lacerda, P., & Luu, J. 2006, *AJ*, 131, 2314
- Lacerda, P., & Jewitt, D. C. 2007, *AJ*, 133, 1393
- Lacerda, P. 2011, *AJ*, 142, 90
- Lacerda, P., McNeill, A., & Peixinho, N. 2014, *MNRAS*, 437, 3824
- Leone, G., Paolicchi, P., Farinella, P., & Zappala, V. 1984, *A&A*, 140, 265
- Levine, S. E., Bida, T. A., Chylek, T., et al. 2012, *Proc. SPIE*, 8444, 844419
- Levison, H. F., & Stern, S. A. 2001, *AJ*, 121, 1730
- Levison, H. F., Morbidelli, A., Van Laerhoven, C., Gomes, R., & Tsiganis, K. 2008, *Icarus*, 196, 258
- Lomb, N. R. 1976, *Ap&SS*, 39, 447
- Malhotra, R. 1993, *Nature*, 365, 819
- Malhotra, R. 1995, *AJ*, 110, 420
- Nesvorný, D., Youdin, A. N., & Richardson, D. C. 2010, *AJ*, 140, 785
- Noll, K. S., Grundy, W. M., Chiang, E. I., Margot, J.-L., & Kern, S. D. 2008, *The Solar System Beyond Neptune*, 345
- Ortiz, J. L., Gutiérrez, P. J., Casanova, V., & Sota, A. 2003, *A&A*, 407, 1149
- Ortiz, J. L., Gutiérrez, P. J., Santos-Sanz, P., Casanova, V., & Sota, A. 2006, *A&A*, 447, 1131
- Peixinho, N., Lacerda, P., & Jewitt, D. 2008, *AJ*, 136, 1837
- Perna, D., Dotto, E., Barucci, M. A., et al. 2009, *A&A*, 508, 451
- Porter, S. B., & Grundy, W. M. 2012, *Icarus*, 220, 947
- Porter, S. B., Spencer, J. R., Benecchi, S., et al. 2016, *ApJ*, 828, L15
- Press, W. H., Teukolsky, S. A., Vetterling, W. T., & Flannery, B. P. 1992, Cambridge: University Press, c1992, 2nd ed.

- Rabinowitz, D. L., Schaefer, B. E., & Tourtellotte, S. W. 2007, *AJ*, 133, 26
- Rabinowitz, D., Schwamb, M. E., Hadjiyska, E., Tourtellotte, S., & Rojo, P. 2013, *AJ*, 146, 17
- Romanishin, W., & Tegler, S. C. 1999, *Nature*, 398, 129
- Rousselot, P., & Petit, J. 2010, *AAS/Division for Planetary Sciences Meeting Abstracts #42*, 42, 40.19
- Schaefer, B. E., & Rabinowitz, D. L. 2002, *Icarus*, 160, 52
- Sheppard, S. S., & Jewitt, D. C. 2002, *AJ*, 124, 1757
- Sheppard, S. S., & Jewitt, D. C. 2003, *Earth Moon and Planets*, 92, 207
- Sheppard, S. S. 2004, Ph.D. Thesis, University of Hawaii.
- Sheppard, S. S., & Jewitt, D. 2004, *AJ*, 127, 3023
- Sheppard, S. S. 2007, *AJ*, 134, 787
- Sheppard, S. S., Lacerda, P., & Ortiz, J. L. 2008, *The Solar System Beyond Neptune*, 129
- Sheppard, S. S. 2012, *AJ*, 144, 169
- Sheppard, S. S., Ragozzine, D., & Trujillo, C. 2012, *AJ*, 143, 58
- Smith, J. A., Tucker, D. L., Kent, S., et al. 2002, *AJ*, 123, 2121
- Snodgrass, C., Carry, B., Dumas, C., & Hainaut, O. 2010, *A&A*, 511, A72
- Stellingwerf, R. F. 1978, *ApJ*, 224, 953
- Stetson, P. B. 1987, *PASP*, 99, 191
- Stetson, P. B. 1990, *PASP*, 102, 932
- Tegler, S. C., Romanishin, W., Stone, A., et al. 1997, *AJ*, 114, 1230
- Thirouin, A., Ortiz, J. L., Duffard, R., et al. 2010, *A&A*, 522, A93
- Thirouin, A., Ortiz, J. L., Campo-Bagatin, A., et al. 2012, *MNRAS*, 424, 3156
- Thirouin, A. 2013, Ph.D. Thesis, University of Granada.
- Thirouin, A., Noll, K. S., Ortiz, J. L., & Morales, N. 2014, *A&A*, 569, A3
- Thirouin, A., Sheppard, S. S., Noll, K. S., et al. 2016, *AJ*, 151, 148
- Thirouin, A., Sheppard, S. S., & Noll, K. S. 2017, *ApJ*, 844, 135
- Thirouin, A., & Sheppard, S. S. 2017, *AJ*, 154, 241
- Trilling, D. E., & Bernstein, G. M. 2006, *AJ*, 131, 1149
- Vilenius, E., Kiss, C., Müller, T., et al. 2014, *A&A*, 564, A35
- Weidenschilling, S. J. 1980, *Icarus*, 44, 80
- Williams, I. P., O’Ceallaigh, D. P., Fitzsimmons, A., & Marsden, B. G. 1995, *Icarus*, 116, 180

This 2-column preprint was prepared with the AAS L^AT_EX macros v5.2.

Table 1: UT-Dates, heliocentric and geocentric (r_h , Δ respectively) distances and phase angle (α , in degrees) are summarized.

Object	UT-date	Nb. of images	r_h [AU]	Δ [AU]	α [°]	Filter	Telescope
1995 HM ₅	05/20/2017	9	29.656	28.647	0.2	VR	DCT
(469362) 2001 KB ₇₇	06/18/2017	6	28.731	27.750	0.5	VR	DCT
2006 UZ ₁₈₄	11/30/2015	6	31.029	30.076-30.077	0.5	VR	DCT
	12/01/2015	4	31.030	30.082	0.5	VR	DCT
2014 JL ₈₀	05/28/2017	10	28.563	27.578	0.5	VR	DCT
	05/29/2017	18	28.563	27.581-27.582	0.5	VR	DCT
	06/18/2017	7	28.559	27.706-27.707	1.1	VR	DCT
	06/28/2017	6	28.557	27.806-27.807	1.4	VR	DCT
2014 JK ₈₀	06/27/2017	4	35.236	34.446-34.447	1.1	VR	DCT
	06/28/2017	6	35.235	34.454-34.455	1.1	VR	DCT
2014 JO ₈₀	06/18/2017	13	31.938-31.939	31.008-31.009	0.7	VR	DCT
	06/27/2017	4	31.945	31.078-31.079	1.0	VR	DCT
	06/28/2017	12	31.946	31.086-31.087	1.0	VR	DCT
	07/02/2017	13	31.949	31.124-31.126	1.1	VR	DCT
2014 JP ₈₀	06/27/2017	5	42.207	41.349	0.7	VR	DCT
2014 JQ ₈₀	05/01/2017	23	31.627	30.670-30.669	0.6	VR	DCT
	05/20/2017	17	31.633	30.627-30.628	0.2	VR	DCT
	05/28/2017	20	31.635	30.641-30.642	0.4	VR	DCT
	05/29/2017	10	31.636	30.644-30.645	0.4	VR	DCT
	06/18/2017	7	31.642	30.762-30.764	0.9	VR	DCT
	06/27/2017	6	31.645	30.850-30.851	1.2	VR	DCT
2014 JT ₈₀	06/27/2017	5	32.245	31.302-31.303	0.7	VR	DCT
2014 KC ₁₀₂	06/18/2017	4	30.505	29.526	0.5	VR	DCT
	07/02/2017	15	30.498	29.581-29.582	0.8	VR	DCT
2014 KX ₁₀₁	05/28/2017	12	31.153	30.143	0.1	VR	DCT
	05/29/2017	5	31.154	30.142	0.1	VR	DCT
2015 BA ₅₁₉	05/01/2017	16	31.041	30.053	0.4	VR	DCT

Table 2: Summary of this work. We report the preferred rotational period (P in h), the full lightcurve amplitude (Δm in mag.), and the Julian Date (φ_0 , no light time correction) corresponding to the zero phase. Absolute magnitude (H), and the diameter considering an albedo of 0.04/0.2 are also indicated.

Object	P [h]	Δm [mag]	φ_0 [JD] [2450000+]	H [mag]	Diameter [km]	Contact binary?
1995 HM ₅	>0.6	>0.1	7893.81062	7.7	192/86	
(469362) 2001 KB ₇₇	>4	>0.15	7922.69978	7.4	220/98	
2006 UZ ₁₈₄	>2	>0.2	7356.78287	7.4	220/98	
2014 JK ₈₀	>1	>0.17	7931.71324	6.1	400/179	
2014 JL ₈₀	34.87	0.55±0.03	7901.76240	7.1	253/113	Likely
2014 JO ₈₀	6.32	0.60±0.05	7922.51572	7.4	220/98	Likely
2014 JP ₈₀	>0.5	>0.1	7931.85876	4.9	696/311	
2014 JQ ₈₀	12.16	0.76±0.04	7874.74484	7.0	265/118	Likely
2014 JT ₈₀	>0.8	>0.1	7931.76831	7.1	253/113	
2014 KC ₁₀₂	>4.5	>0.2	7922.70464	7.1	253/113	
2014 KX ₁₀₁	>3	>0.2	7901.78398	7.4	220/98	
2015 BA ₅₁₉	>4/8 ^a	~0.16	7874.73116	7.4	220/98	

Notes:

In case of partial lightcurve, the lower limit to the period reported is the duration of our observing block.

^a: The lightcurve of 2015 BA₅₁₉ shows a maximum and minimum over about 4 h of observations. Therefore, the rotational period of this object is likely >8 h (double-peaked).

TABLE 3

SHORT-TERM VARIABILITY OF THE PLUTINO TRANS-NEPTUNIAN OBJECTS IS SUMMARIZED. PREFERRED ROTATIONAL PERIOD IS INDICATED IN BOLD. REFERENCE LIST IS AFTER THE TABLE.

Object	Single-peaked period [h]	Double-peaked period [h]	Δm [mag]	H [mag]	Ref.
(134340) Pluto	153.2	-	0.33	-0.7	B97
Charon	153.6	-	0.08	0.9	B97
(15789) 1993 SC	7.7129	-	0.5	7.0	W95
(15810) 1994 JR ₁ Arawn	-	-	<0.2	...	T97, D97 ^a
(15820) 1994 TB	-	5.47±0.33	0.58	7.7	P16
(32929) 1995 QY ₉	3.0/3.5	6.0/7.0	0.26/0.34	7.3	RT99
(15875) 1996 TP ₆₆	-	-	<0.04	...	SJ02
(118228) 1996 TQ ₆₆	-	7.3±0.1	0.60±0.04	8.0	RT99,SJ02
(91133) 1998 HK ₁₅₁	1.96	-	<0.04	7.0	CB99 ^b
(33340) 1998 VG ₄₄	-	-	<0.12	...	RT99
(47171) 1999 TC ₃₆	-	-	<0.22	6.9	RT99
(38628) 2000 EB ₁₇₃ Huya	6.21±0.02	-	<0.15	7.6	SJ02
	-	-	<0.10	6.5	SJ02
	-	-	0.06	4.9	O03
	-	-	<0.07	...	LL06
	-	-	<0.05	...	SJ03
	(6.68/6.75/6.82)±0.01	-	<0.1	4.8	O03
	-	-	<0.15	...	SJ02
	-	-	<0.06	...	SR02
	-	-	<0.04	...	SJ03,LL06
	5.21	-	0.02±0.01	...	T14
	4.45±0.07	-	~0.1	...	G16
2000 FV ₅₃	-	7.5	0.07±0.02	8.3	TB06
(47932) 2000 GN ₁₇₁	-	8.329±0.005	0.61±0.03	6.2	SJ02
	-	-	0.53	...	D08 ^c
	-	-	0.64±0.11	...	R07
2001 KD ₇₇	-	-	<0.07	5.8	SJ03
(469372) 2001 QF ₂₉₈	-	-	<0.12	5.2	SJ03
	-	-	~0.11	...	T13
(139775) 2001 QG ₂₉₈	6.8872±0.0002	13.7744±0.0004	1.14±0.04	6.9	SJ04
	-	13.7744±0.0004	0.7±0.01	...	L11
(28978) 2001 KX ₇₆ Ixion	-	-	<0.05	3.6	O03,SJ03
	15.9±0.5	-	0.06±0.03	...	RP10
	12.4±0.3	-	-	...	G16
(55638) 2002 VE ₉₅	(6.76/6.88/7.36/9.47)±0.01	-	0.08±0.04	5.5	O06
	-	-	<0.06	...	SJ03
	9.97	-	0.05±0.01	...	T10
(208996) 2003 AZ ₈₄	(4.32/5.28/6.72/6.76)±0.01	-	0.10±0.04	3.7	O06
	6.72±0.05	-	0.14±0.03	...	SJ03
	6.79	-	0.07±0.01	...	T10
	6.78	-	0.07±0.01	...	T14
2003 HA ₅₇	-	6.44	0.31±0.03	8.1	T16
(455502) 2003 UZ ₄₁₃	-	4.13±0.05	0.13±0.03	4.3	P09
(84922) 2003 VS ₂	(3.71 or 4.39)±0.01	-	0.23±0.07	4.2	O06
	-	7.41±0.02	0.21±0.02	...	S07
	-	7.42	0.21±0.01	...	T10
	-	7.4208	0.224±0.013	...	T13
(90482) 2004 DW Orcus	7.09/10.08±0.01/17.43	20.16	0.04±0.02	2.2	O06
	13.19	-	0.18±0.08	...	R07
	-	-	<0.03	...	S07
	10.47	-	0.04±0.01	...	T10
	11.9±0.5	-	-	...	G16
(469708) 2005 GE ₁₈₇	6.1	-	0.5	7.3	S10
	-	11.99	0.29±0.02	...	T16
(469987) 2006 HJ ₁₂₃	-	-	<0.13	5.9	BS13
(341520) 2007 TY ₄₃₀ Mors-Somnus	-	9.28	0.24±0.05	6.9	T14 ^d

Notes:

^a: Results from Williams et al. (1995) were not supported by Tegler et al. (1997), and Davies et al. (1997). Thus, this object will not be considered in our study. ^b: Rotational period of 1996 TP₆₆ is likely wrong, and will not be used in this work. ^c: Dotto et al.

(2008) used the rotational period from Sheppard & Jewitt (2002) to fit their data. They reported a lightcurve amplitude of 0.60±0.03 mag, but based on their fit (Figure 3 of Dotto et al. (2008)), the lightcurve amplitude is about 0.53 mag. ^d: According to Sheppard et al. (2012), 2007 TY₄₃₀ is dynamically cold classical object in the Plutino population.

References list:

W95: Williams et al. (1995); B97: Buie et al. (1997); D97: Davies et al. (1997); T97: Tegler et al. (1997); CB99: Collander-Brown et al. (1999); RT99: Romanishin & Tegler (1999); SJ02: Sheppard & Jewitt (2002); SR02: Schaefer & Rabinowitz (2002); O03: Ortiz et al. (2003); SJ03: Sheppard & Jewitt (2003); SJ04: Sheppard & Jewitt (2004); LL06: Lacerda & Luu (2006); O06: Ortiz et al. (2006); TB06: Trilling & Bernstein (2006); R07: Rabinowitz et al. (2007); S07: Sheppard (2007); D08: Dotto et al. (2008); P09: Perna et al. (2009); RP10: Rousselot & Petit (2010); S10: Snodgrass et al. (2010); T10: Thirouin et al. (2010); L11: Lacerda (2011); BS13: Benecchi & Sheppard (2013); T13: Thirouin (2013); T14: Thirouin et al. (2014); G16: Galiazzi et al. (2016); P16: Porter et al. (2016); T16: Thirouin et al. (2016).

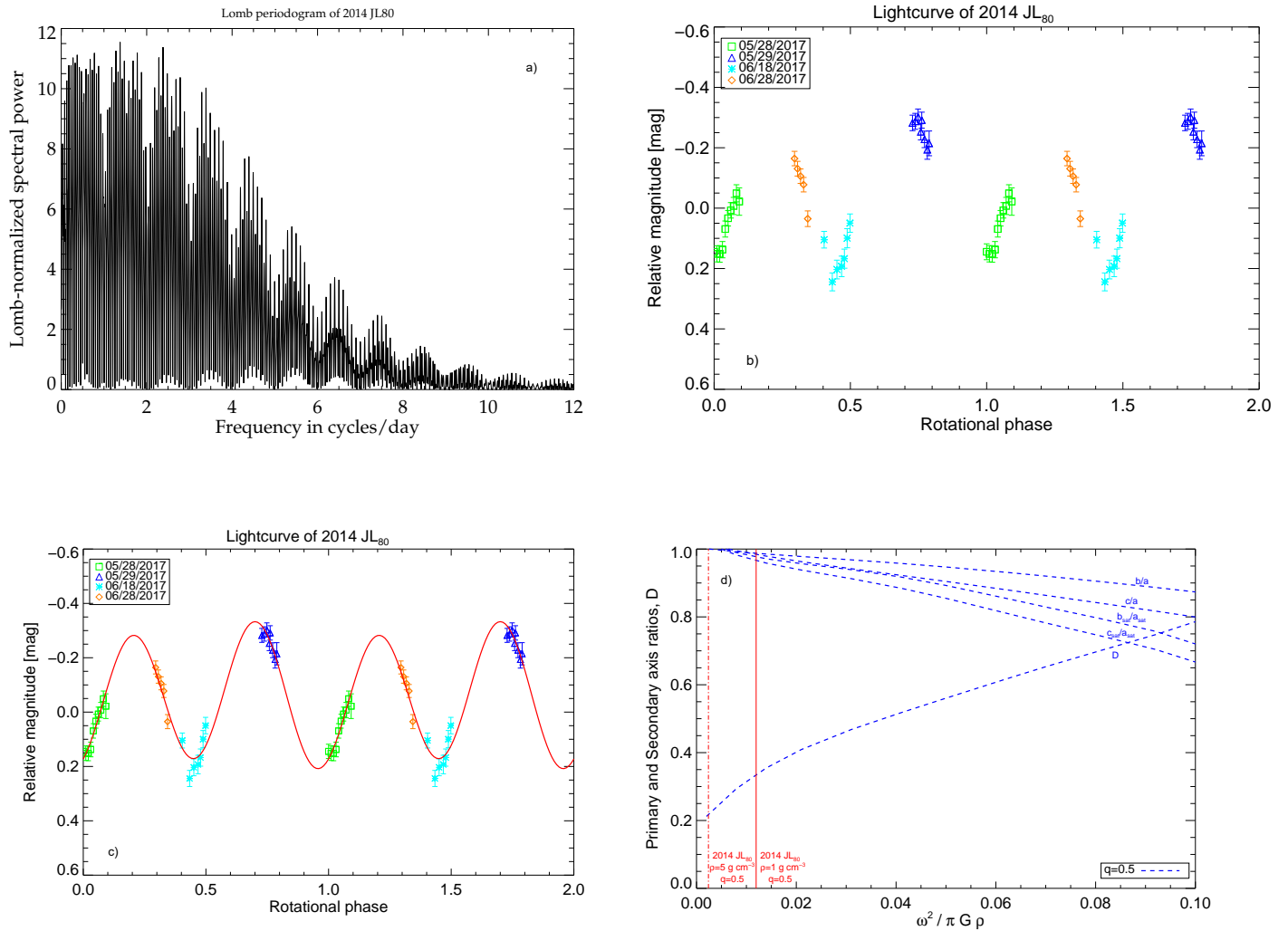


Fig. 1.— *Study of 2014 JL₈₀*: The Lomb periodogram presents several peaks, but the highest one suggests a double-peaked periodicity of 34.87 h (plot a)). The corresponding lightcurve is plotted on plot b). We tried to fit a Fourier Series (2nd order) to our data (red continuous line, plot c)), but the fit failed to reproduce the V-shape of the second minima. Because the lightcurve displays a large variability, and because of the V-shape of the second peak, we suggest that this object is a contact binary. The plot d) was used to derive the basic information of the system, assuming a contact binary nature.

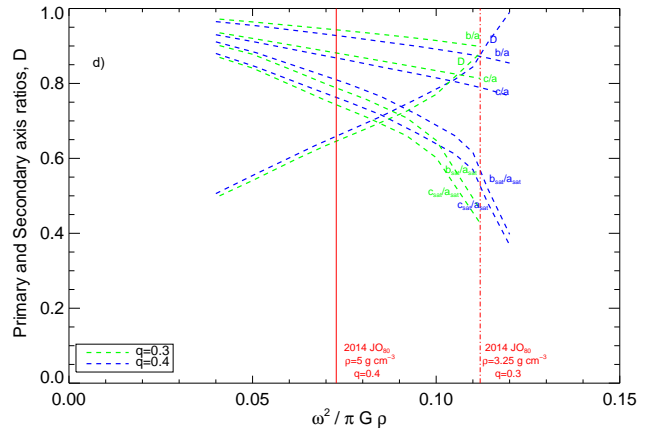
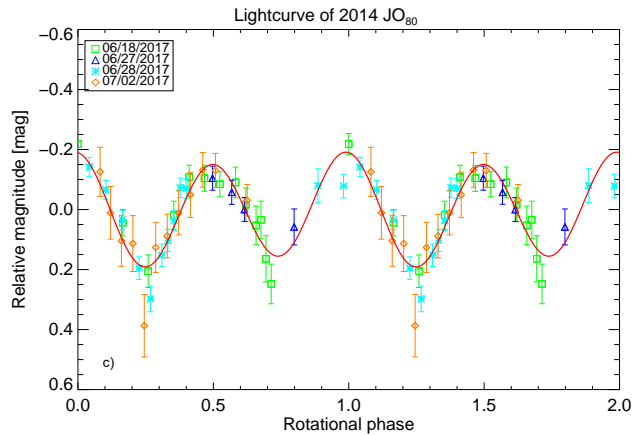
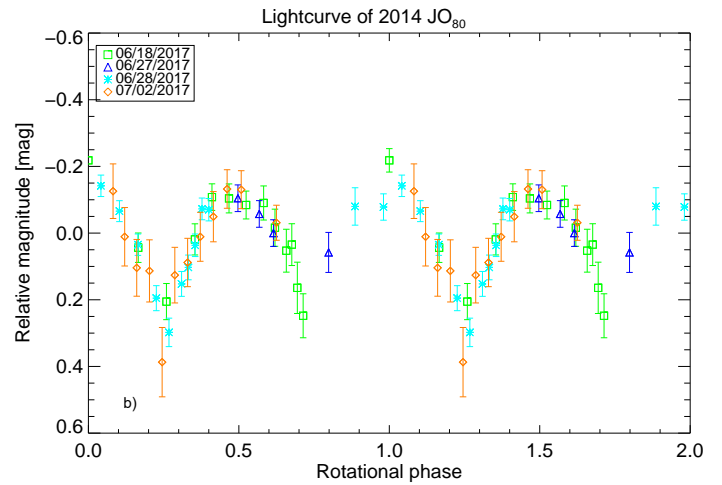
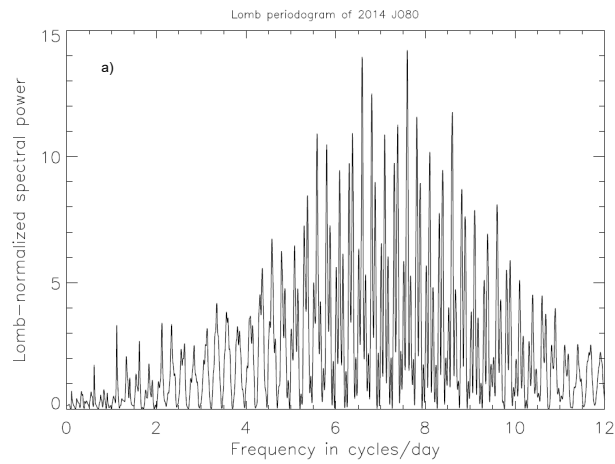


Fig. 2.— *Study of 2014 JO₈₀*: The highest peak of the Lomb periodogram favors a rotational period of 3.16 h (plot a)). However, based on the asymmetry of the lightcurve and the large amplitude, we favor the double-peaked option with a rotational period of 6.32 h (plot b)). A second order Fourier Series fit is not able to reproduce the V- and U-shape of the lightcurve, therefore, we propose that 2014 JO₈₀ is likely a contact binary (plot c)). In order to derive basic information about the system, we used [Leone et al. \(1984\)](#) work and summarized our results in the plot d).

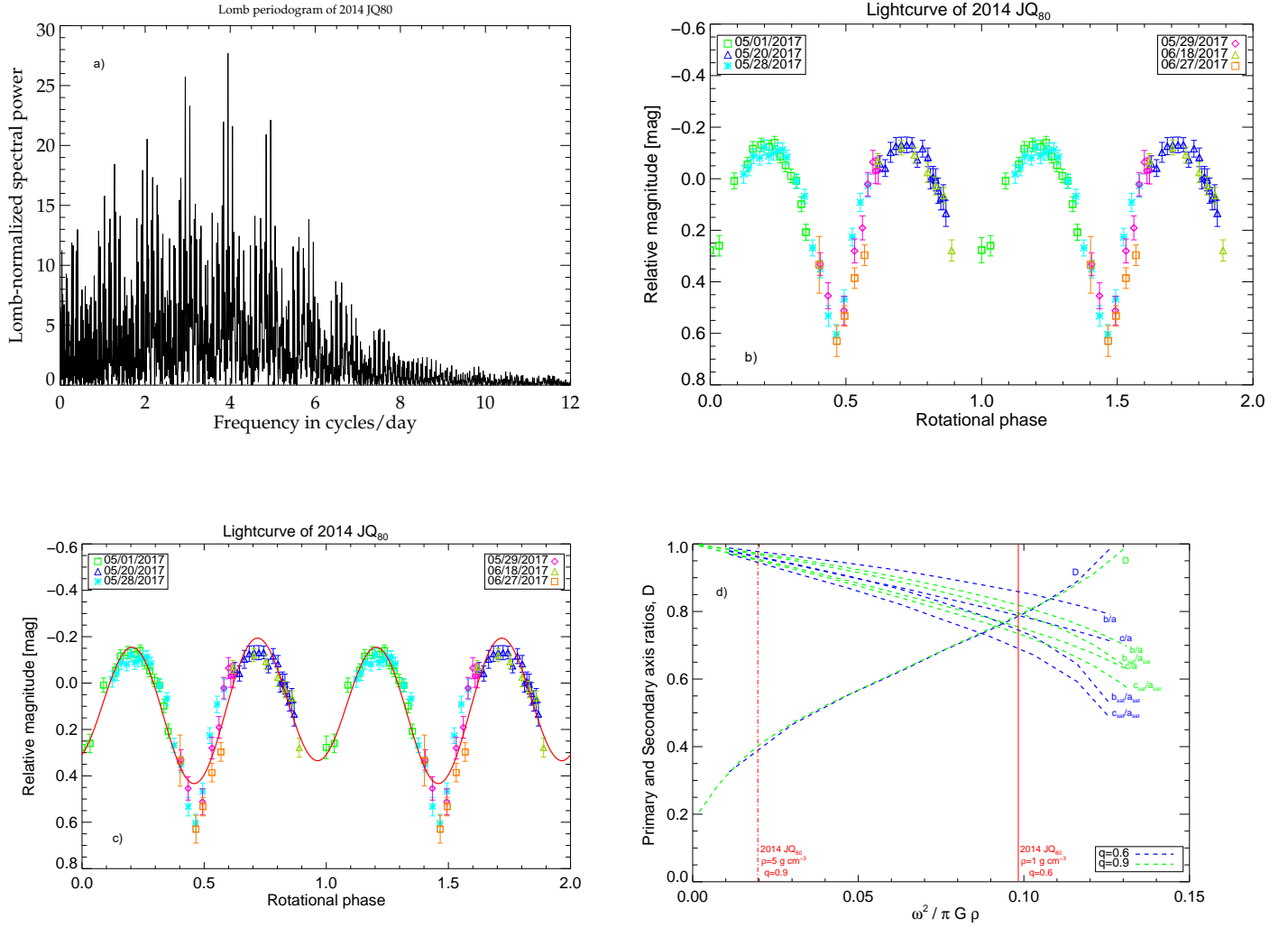


Fig. 3.— *Study of 2014 JQ₈₀*: Based on the Lomb periodogram study, we estimate that 2014 JQ₈₀ has a double-peaked lightcurve with a rotational period of 12.16 h (plot a)). Because the lightcurve displays a large variability, and because of the V-/U-shapes of the minima/maxima, we suggest that this object is a contact binary (plot b), and c)). The plot d) was used to derive the basic information of the system, assuming a contact binary nature.

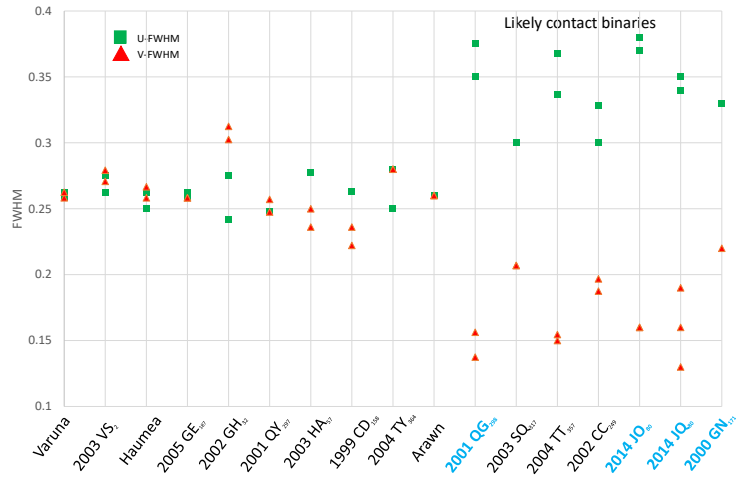


Fig. 4.— *Full width at half maximum (FWHM) of single objects, resolved binaries and (likely/confirmed) contact binaries*: A complete description of this plot is available in [Thirouin & Sheppard \(2017\)](#). The (likely/confirmed) contact binaries present a $U\text{-FWHM} \geq 0.30$, and a $V\text{-FWHM} \leq 0.22$. Likely contact binary in the Plutino population have their name highlighted in light blue. This study made use of lightcurves plotted as magnitude versus rotational phase.

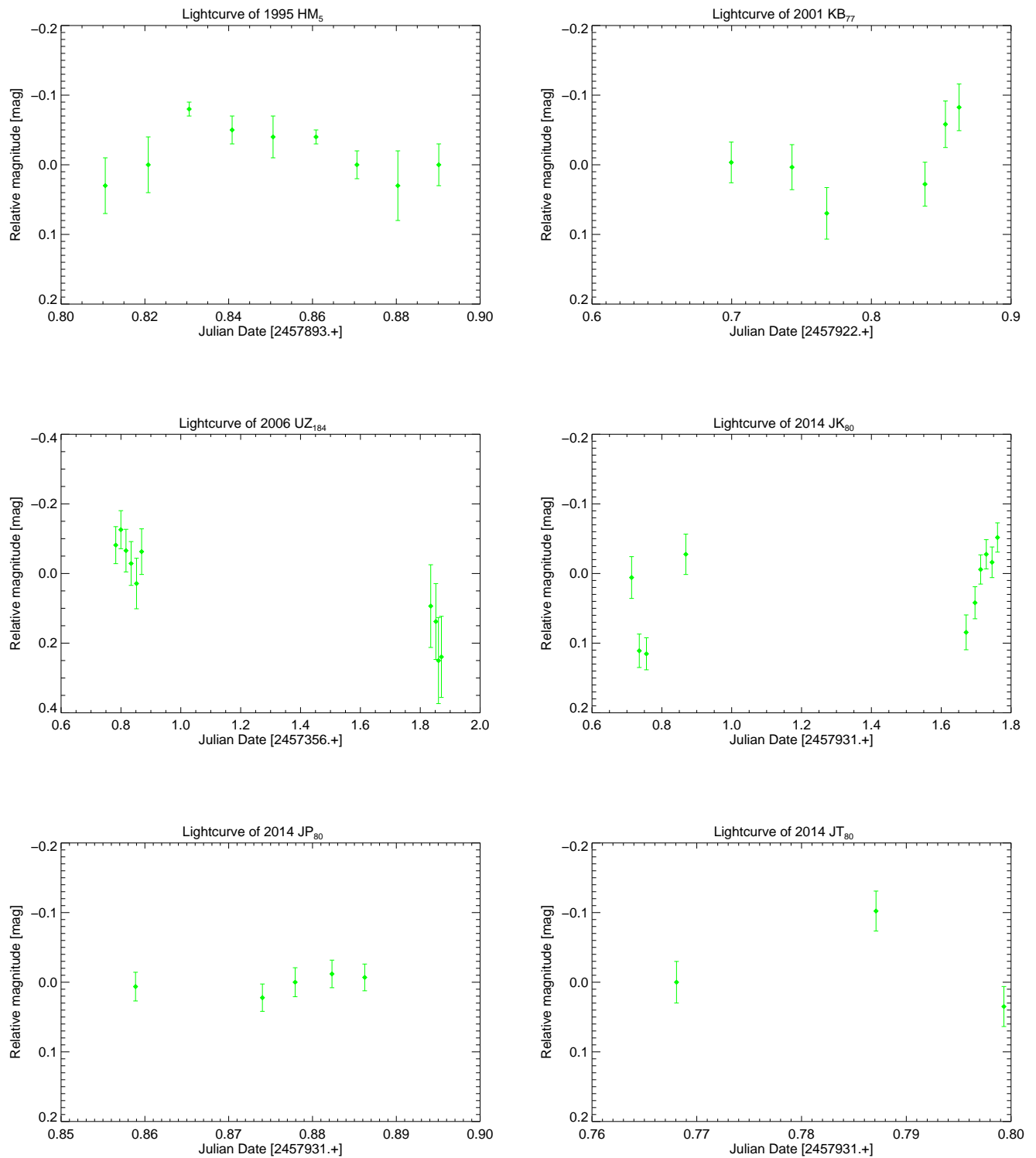


Fig. 5.— *Partial lightcurves of several Plutinos*: we report relative magnitude versus Julian Date (no light-time correction) for nine objects.

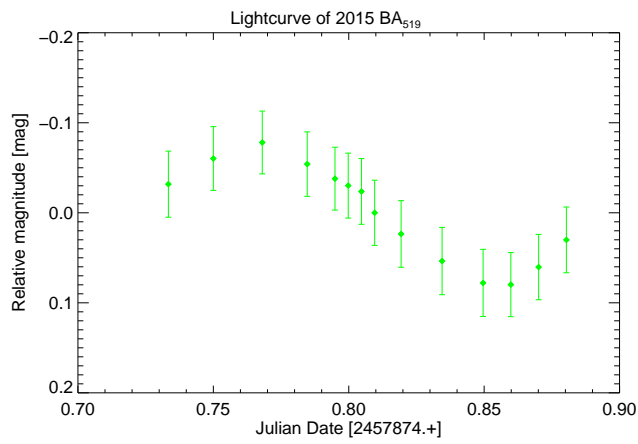
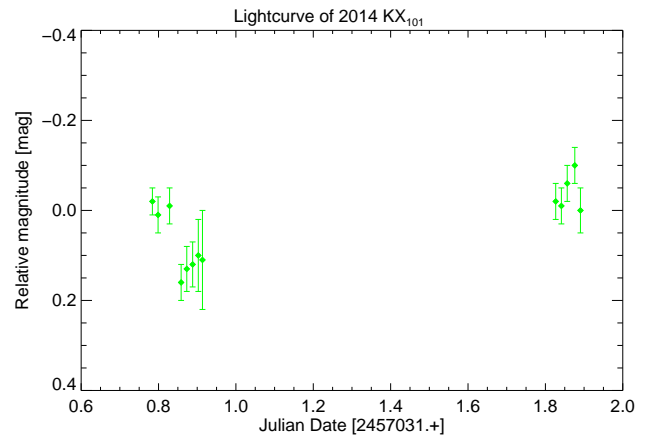
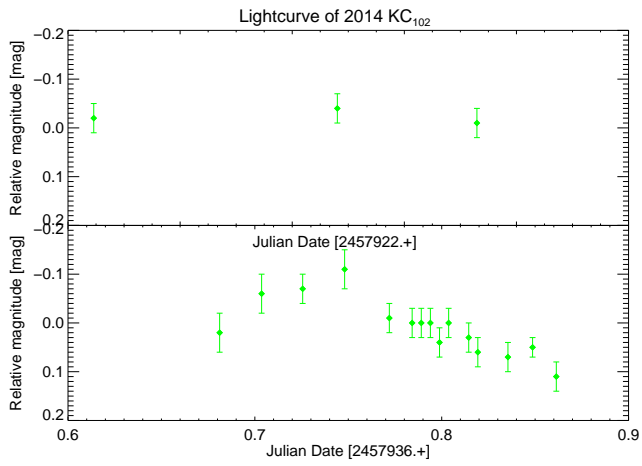


Fig. 6.— *Partial lightcurves of several Plutinos: continuation of Figure 5.*

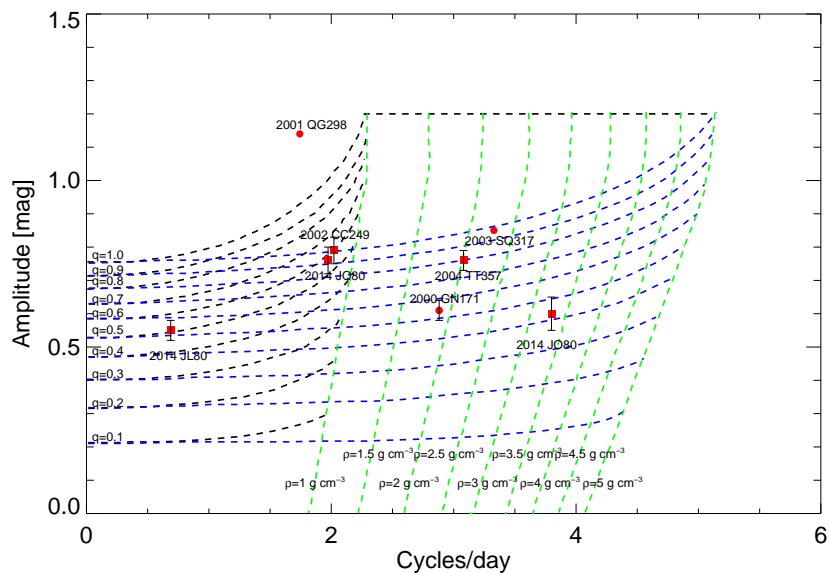


Fig. 7.— *The network of Roche sequences*: A complete description of this plot is available in [Leone et al. \(1984\)](#); [Throuin et al. \(2017\)](#). Confirmed/likely contact binaries from this work and the literature are plotted. Name of each objects is also indicated.

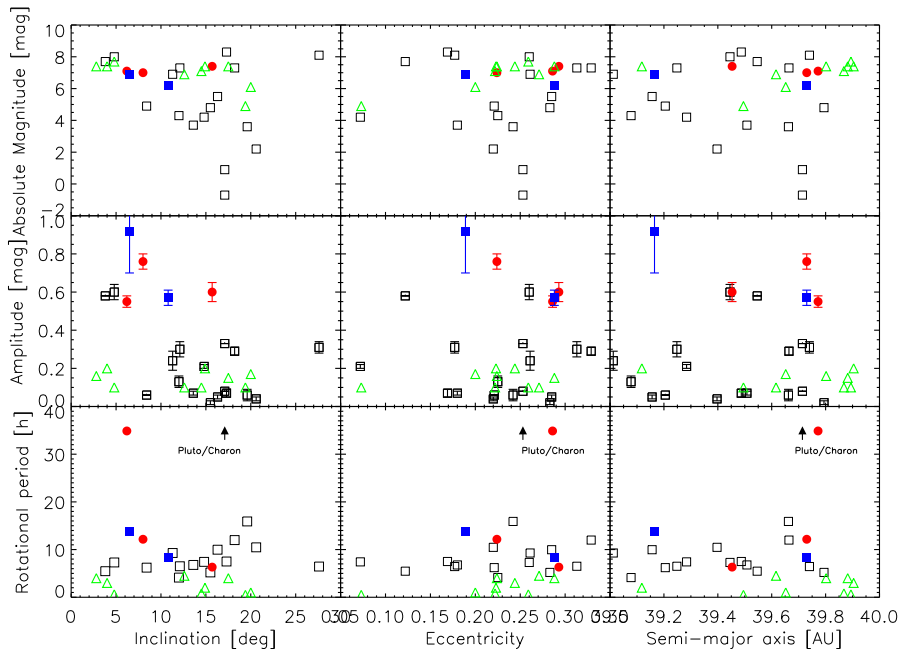
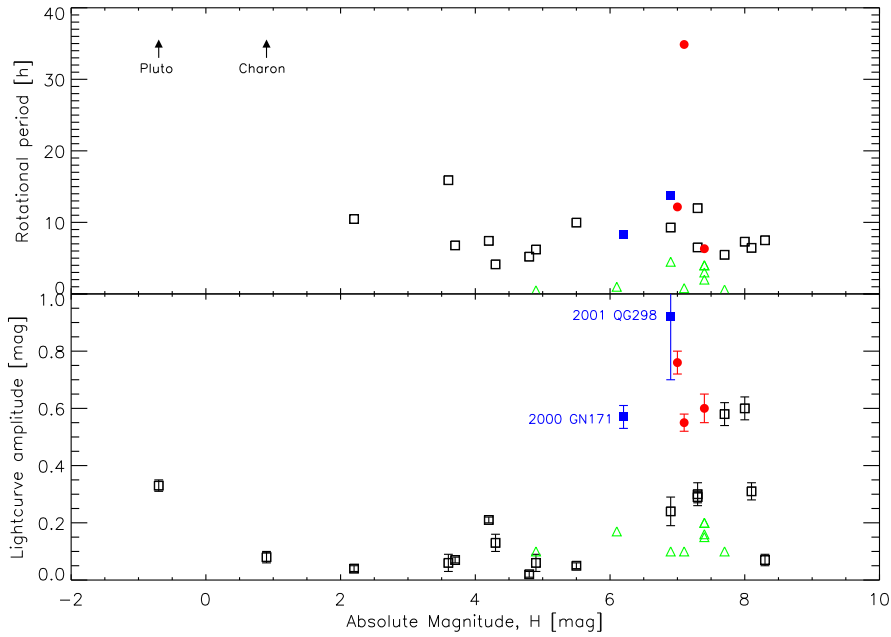


Fig. 8.— *Rotational properties and orbital elements*: All the Plutinos with published lightcurves are plotted. Open black squares are from the literature, green triangles are plutinos with partial lightcurves reported in this work (lower estimates for the period and amplitude), red circles are the likely contact binaries from this work and blue circles are the likely/confirmed contact binaries from the literature. There is a correlation between amplitude and absolute magnitude and an anti-correlation between inclination and lightcurve amplitude.

Appendix A

TABLE 4
 PHOTOMETRY USED IN THIS PAPER IS AVAILABLE IN THE FOLLOWING TABLE.

Object	JD	Rel. mag. [mag]	Err. [mag]
1995 HM ₅	2457893.81062	0.03	0.04
	2457893.82056	0.00	0.04
	2457893.83067	-0.08	0.01
	2457893.84067	-0.05	0.02
	2457893.85073	-0.04	0.03
	2457893.86061	-0.04	0.01
	2457893.87065	0.00	0.02
	2457893.88050	0.03	0.05
	2457893.89038	0.00	0.03
2001 KB ₇₇	2457922.69978	0.00	0.03
	2457922.74331	0.00	0.03
	2457922.76815	0.07	0.04
	2457922.83814	0.03	0.03
	2457922.85305	-0.06	0.03
	2457922.86298	-0.08	0.03
2006 UZ ₁₈₄	2457356.78287	-0.08	0.05
	2457356.79985	-0.13	0.05
	2457356.81682	-0.07	0.06
	2457356.83377	-0.03	0.06
	2457356.85215	0.03	0.07
	2457356.86895	-0.06	0.07
	2457357.83488	0.09	0.12
	2457357.85205	0.14	0.11
	2457357.86094	0.25	0.12
	2457357.87037	0.24	0.12
2014 JL ₈₀	2457901.76402	0.14	0.03
	2457901.77899	0.15	0.03
	2457901.79376	0.15	0.03
	2457901.80857	0.14	0.03
	2457901.82354	0.07	0.03
	2457901.83837	0.03	0.03
	2457901.85321	0.01	0.03
	2457901.86809	-0.01	0.03
	2457901.88304	-0.05	0.03
	2457901.89786	-0.02	0.05

TABLE 4—*Continued*

Object	JD	Rel. mag. [mag]	Err. [mag]
	2457902.82155	-0.28	0.03
	2457902.83643	-0.29	0.03
	2457902.85129	-0.30	0.03
	2457902.86610	-0.25	0.03
	2457902.87091	-0.29	0.03
	2457902.88573	-0.23	0.03
	2457902.90052	-0.19	0.03
	2457902.91029	-0.21	0.04
	2457922.68985	0.10	0.03
	2457922.73343	0.24	0.03
	2457922.75813	0.20	0.03
	2457922.78302	0.19	0.03
	2457922.79789	0.17	0.03
	2457922.81280	0.10	0.03
	2457922.82776	0.05	0.03
	2457932.70192	-0.16	0.02
	2457932.71803	-0.13	0.02
	2457932.73411	-0.11	0.02
	2457932.75037	-0.08	0.02
	2457932.77251	0.04	0.03
<hr/>			
2014 JK ₈₀			
	2457931.71324	0.01	0.03
	2457931.73529	0.11	0.02
	2457931.75585	0.12	0.02
	2457931.86866	-0.03	0.03
	2457932.67154	0.08	0.03
	2457932.69694	0.04	0.02
	2457932.71301	-0.01	0.02
	2457932.72915	-0.03	0.02
	2457932.74536	-0.02	0.02
	2457932.76141	-0.05	0.02
<hr/>			
2014 JO ₈₀			
	2457922.51572	-0.22	0.04
	2457922.55931	0.04	0.04
	2457922.58397	0.21	0.05
	2457922.60888	0.02	0.05
	2457922.62380	-0.11	0.04
	2457922.63871	-0.10	0.04
	2457922.65367	-0.08	0.04

TABLE 4—*Continued*

Object	JD	Rel. mag. [mag]	Err. [mag]
	2457922.66899	-0.09	0.05
	2457922.67890	-0.02	0.06
	2457922.68883	0.05	0.06
	2457922.69364	-0.03	0.06
	2457922.69845	0.16	0.08
	2457922.70355	0.02	0.07
	2457931.59498	-0.10	0.04
	2457931.61365	-0.06	0.04
	2457931.62604	0.00	0.04
	2457931.67432	0.06	0.06
	2457932.48703	-0.08	0.06
	2457932.51189	-0.08	0.04
	2457932.52791	-0.14	0.03
	2457932.54409	-0.11	0.03
	2457932.56027	0.03	0.03
	2457932.57636	0.20	0.04
	2457932.58742	0.30	0.04
	2457932.59845	0.22	0.04
	2457932.60441	0.17	0.04
	2457932.61036	0.04	0.03
	2457932.61633	-0.07	0.03
	2457932.62227	-0.07	0.03
	2457936.48638	-0.18	0.08
	2457936.49655	0.01	0.09
	2457936.50709	0.10	0.09
	2457936.51822	0.11	0.09
	2457936.52931	0.39	0.10
	2457936.54040	0.13	0.08
	2457936.55159	0.09	0.07
	2457936.56266	0.11	0.07
	2457936.57412	-0.02	0.08
	2457936.58614	-0.13	0.06
	2457936.59847	-0.18	0.06
	2457936.62931	-0.23	0.05
2014 JP ₈₀			
	2457931.85879	0.01	0.02
	2457931.87378	0.02	0.02
	2457931.87801	0.00	0.02
	2457931.88222	-0.01	0.02

TABLE 4—*Continued*

Object	JD	Rel. mag. [mag]	Err. [mag]
	2457931.88645	-0.01	0.02
2014 JQ ₈₀			
	2457874.56771	0.28	0.05
	2457874.58431	0.26	0.04
	2457874.61256	0.01	0.03
	2457874.63733	-0.06	0.03
	2457874.64747	-0.12	0.03
	2457874.66268	-0.13	0.03
	2457874.67782	-0.12	0.02
	2457874.68806	-0.14	0.02
	2457874.69826	-0.09	0.03
	2457874.70837	-0.05	0.03
	2457874.71855	-0.01	0.03
	2457874.72859	0.01	0.03
	2457874.73764	0.10	0.03
	2457874.74648	0.21	0.03
	2457893.63097	-0.06	0.03
	2457893.64101	-0.04	0.03
	2457893.65111	-0.10	0.04
	2457893.66115	-0.13	0.03
	2457893.67116	-0.19	0.03
	2457893.68113	-0.21	0.03
	2457893.69109	-0.25	0.03
	2457893.70102	-0.17	0.03
	2457893.71090	-0.17	0.03
	2457893.72083	-0.08	0.04
	2457893.72562	0.00	0.04
	2457893.73051	-0.01	0.04
	2457893.73529	0.00	0.04
	2457893.74010	0.05	0.05
	2457893.74489	0.08	0.04
	2457893.74970	0.07	0.05
	2457893.75449	0.13	0.05
	2457901.48354	-0.02	0.03
	2457901.49326	-0.04	0.03
	2457901.50170	-0.09	0.03
	2457901.51366	-0.08	0.03
	2457901.52225	-0.12	0.03
	2457901.53065	-0.19	0.03

TABLE 4—*Continued*

Object	JD	Rel. mag. [mag]	Err. [mag]
	2457901.53909	-0.10	0.03
	2457901.54762	-0.11	0.03
	2457901.55603	-0.11	0.03
	2457901.56440	-0.08	0.03
	2457901.58213	0.01	0.03
	2457901.59716	0.07	0.03
	2457901.61194	0.27	0.03
	2457901.62676	0.35	0.03
	2457901.64163	0.53	0.04
	2457901.65651	0.51	0.04
	2457901.67137	0.47	0.04
	2457901.68621	0.23	0.03
	2457901.70116	0.09	0.04
	2457901.71594	0.03	0.04
	2457902.63970	0.33	0.04
	2457902.65451	0.45	0.05
	2457902.68421	0.51	0.06
	2457902.70386	0.28	0.05
	2457902.71862	0.21	0.05
	2457902.72843	0.02	0.05
	2457902.73822	-0.06	0.05
	2457902.74311	-0.03	0.05
	2457902.74794	-0.03	0.05
	2457922.50729	-0.17	0.03
	2457922.55085	-0.12	0.03
	2457922.57560	-0.09	0.03
	2457922.60046	0.12	0.04
	2457922.61527	0.13	0.04
	2457922.63021	-0.06	0.03
	2457922.64512	0.28	0.04
	2457931.51794	0.33	0.11
	2457931.52869	0.74	0.12
	2457931.55075	0.63	0.06
	2457931.56522	0.53	0.04
	2457931.58388	0.44	0.04
	2457931.60254	0.32	0.04
2014 JT ₈₀			
	2457931.76831	0.00	0.03
	2457931.78695	-0.10	0.03

TABLE 4—*Continued*

Object	JD	Rel. mag. [mag]	Err. [mag]
	2457931.79933	0.03	0.03
2014 KC ₁₀₂	2457922.70464	-0.02	0.03
	2457922.74820	-0.04	0.03
	2457922.77305	-0.01	0.03
	2457936.68128	0.02	0.04
	2457936.70355	-0.06	0.04
	2457936.72572	-0.07	0.03
	2457936.74803	-0.11	0.04
	2457936.77202	-0.01	0.03
	2457936.78435	0.00	0.03
	2457936.78916	0.00	0.03
	2457936.79394	0.00	0.03
	2457936.79875	0.04	0.03
	2457936.80354	0.00	0.03
	2457936.81460	0.03	0.03
	2457936.81941	0.06	0.03
	2457936.83553	0.07	0.03
	2457936.84842	0.05	0.02
	2457936.86129	0.11	0.03
2014 KX ₁₀₁	2457901.78398	-0.02	0.03
	2457901.79876	0.01	0.04
	2457901.82852	-0.01	0.04
	2457901.85819	0.16	0.04
	2457901.87313	0.13	0.05
	2457901.88802	0.12	0.05
	2457901.90293	0.10	0.08
	2457901.91350	0.11	0.11
	2457902.82649	-0.02	0.04
	2457902.84142	-0.01	0.04
	2457902.85625	-0.06	0.04
	2457902.87591	-0.10	0.04
	2457902.89068	0.00	0.05
2015 BA ₅₁₉	2457874.73348	-0.03	0.04
	2457874.74995	-0.06	0.04
	2457874.76792	-0.08	0.03
	2457874.78450	-0.05	0.04

TABLE 4—*Continued*

Object	JD	Rel. mag. [mag]	Err. [mag]
	2457874.79498	-0.04	0.03
	2457874.79977	-0.03	0.04
	2457874.80458	-0.02	0.04
	2457874.80936	0.00	0.04
	2457874.81954	0.02	0.04
	2457874.83469	0.05	0.04
	2457874.84984	0.08	0.04
	2457874.86009	0.08	0.04
	2457874.87030	0.06	0.04
	2457874.88044	0.03	0.04
	2457874.90070	0.00	0.04